Journal of the Indian Chemical Society 99 (2022) 100437

Contents lists available at ScienceDirect

Journal of the Indian Chemical Society

journal homepage: www.journals.elsevier.com/journal-of-the-indian-chemical-society

Spectroscopic investigations (FTIR, UV-VIS, NMR) and DFT calculations on the molecular structure of N_ω-Nitro-L-arginine

A. Mary Girija [a,b], M.M. Armstrong Arasu [b,*], D. Devi [a,b]

[a] PG & Research Department of Physics, Cauvery College for Women (Autonomous), Tiruchirappalli, 620 018, TN, India
[b] Department of Physics, St. Joseph's College (Autonomous) (Affiliated to Bharathidasan University), Tiruchirappalli, 620002, TN, India

ARTICLE INFO

Keywords:
FT-IR
HOMO LUMO
N_ω-nitro-L-arginine
NMR
Corrosion inhibitors

ABSTRACT

The spectroscopic properties of N_ω-nitro-L-arginine were investigated by FT-IR, UV-VIS, and ^{1}H NMR spectra. Geometrical parameters and energies were calculated using the density functional theory (DFT) B3LYP method with the 6-311G basis set. Geometrical optimization of the molecule has been performed, vibrational spectra have been calculated, and fundamental vibrations have been determined from the total energy distribution (TED) of the vibrational modes. The HOMO-LUMO analysis is carried out for various electric fields (0.0–0.025 A^{-1}). The HOMO-LUMO gap is decreased while increasing the electric field. The calculated quantum chemical parameters are calculated and correlated to the inhibition efficiency, A Mullliken population was also important for determining local reactivity by indicating reactive centers and identifying potential nucleophilic and electrophilic attack sites. Charge transfer occurs inside the compound based on the HOMO LUMO gap. Calculations of DFT were evaluated in their ability to predict inhibition efficiency.

1. Introduction

The origin of amino acids is protein. It consists of an amino group and a carboxylic group [1]. The various applications in the industry amino acids are used [2]. The chelating ability of amino acids is used in agricultural fertilizers and these fertilizers are used to prevent possible deficiencies and to improve plant life. In combination with drugs and cosmetics some types of amino acids are used. Likewise, some amino acid derivatives are used in the pharmaceutical industry. One of the basic amino acid is L-arginine (L-Arg) and it is encoded by DNA [3]. L-arginine is a well-known organic compound from the amino acid family with good structural flexibility because it exists in 3 zwitter ionic forms, with protonation of guanidyl, alpha amino group and deprotonation of carboxyl groups. Owing to these characteristic properties L-arginine makes interaction with other salts much easier to form inter and intra molecular interactions, such as hydrogen bonds and ionic bonds.

The presence of these interactions and the high structural flexibility of L-arginine provide a variety of molecular conformations of their compounds [4–7]. Nitroarginine, or N_ω-nitro-L-arginine, also known as L-NOARG, is a nitro derivative of the amino acid arginine [8]. Thus, in the study of nitric oxide and its biological effects, it is widely used as a biochemical tool [9,10]. Corrosion of metals is a major industrial problem that has generated a great deal of research and investigation. The use of inhibitors is one of the most effective ways to protect metals from corrosion. DFT is easy to identify the molecular active sites and also to predict the inhibition efficiency trends. Amino acids play a major role in corrosion inhibitors.

Owing to the many applications of the title compound, the current study focuses on molecular geometry, optimized parameters and vibrational frequencies of N_ω-nitro- L-arginine as well as the computational approaches (B3LYP) at the 6-311G basis set. Therefore, the molecular structure of N-NLA is investigated in the current study using density functional theory. The focus also extends to a complete description of molecular geometry, the vibrational frequencies, HOMO–LUMO energies, isotropic chemical shifts, and the excitation energy of N-NLA. For an understanding of reactive nature of the compound, the global reactivity descriptors, namely, hardness (η), softness (s), chemical potential (μ), ionization energy (I), electron affinity (A), absolute electronegativity (χ), the fraction of electron transferred (ΔN) and the electrophilicity index (ω) are also calculated. Fukui indices have been used to analyze the local reactivity, since they represent the nucleophilic and electrophilic behavior of each atom within the molecule. The first hyperpolarizability is also studied using the DFT/B3LYP

* Corresponding author.
E-mail address: armstrongarasu@gmail.com (M.M.A. Arasu).

https://doi.org/10.1016/j.jics.2022.100437
Received 8 December 2021; Received in revised form 28 January 2022; Accepted 18 March 2022
Available online 22 March 2022

Table 1
Optimized parameters of Nω-Nitro-L-Arginine using B3LYP/6-311G method.

Bond Length	Values[a](Å)	Exp[a]	Bond Angle	Values (°)	Exp[a]	Dihedral Angle	Values (°)	Exp[a]
O1 –C14	1.3822	1.3510	C14–O1–H25	110.5754	110	H25–O1–C14–O2	1.4909	–
O1–H25	0.9783	0.8400	C12–N5–H23	113.8394	115.4	H25–O1–C14–C12	−178.021	−124.7
O2–C 14	1.2318	1.3510	C12–N5–H24	112.6872	115.4	H23–N5–C12–H14	70.6354	–
O3–N 9	1.2648	1.2370	H23–N5–H24	110.7045	107	H23–N5–C12–H20	−48.1861	–
O 4-N 9	1.2754	1.2370	C13–N6–C15	120.1865	122.47	H24–N5–C12–H20	−175.319	−124.7
N 5-C 12	1.4631	1.4920	N9–N7–C15	130.2171	–	C15–N6–C13–C11	179.3278	172.3
N5–H 23	1.0122	0.9900	N9–N7–H26	114.0713	–	C15–N6–C13–H22	−60.1831	–
N5–H 24	1.0133	0.9900	C15–N7–H26	115.7113	115.4	C13–N6–C15–N8	−0.2661	–
N6– C13	1.4694	1.4718	C15–N8–H27	119.478	120.1	C15–N7–N9–O4	−0.1609	–
N6 –C15	1.2873	1.04724	C15–N8–H28	120.2858	120.1	H26–N7–N9–O4	−179.9501	–
N7 –N9	1.3701	–	H27–N8–C28	120.2357	–	N9–N7–C15–N6	−179.7105	–
N7–C 15	1.4283	1.4718	O3–N9–O4	124.854	120.7	N9–N7–C15–N8	0.2207	–
N7–H26	1.01	0.9600	O3–N9–N7	115.8274	–	H26–N7–C15–N8	180.0071	–
N8–C 15	1.3644	0.8600	O4–N9–N7	119.3186	–	H27–N8–C15–N6	−0.2691	–
N8–H 27	1.0022	0.9900	C11–C10–C12	115.3431	116.35	H27–N8–C15–N7	179.8132	–
N8–H 28	1.0069	0.99	C11–C10–H16	109.1688	109.9	H28–N8–C15–N7	0.048	–
C10–C 11	1.5345	1.5240	C11–C10–H17	110.2107	109.9	C12–C10–C11–C13	178.8732	–
C10–C 12	1.5487	1.5240	C12–C10–H16	108.994	109.9	C12–C10–C11–H19	57.7565	–
C10–H 16	1.0929	0.93	C12–C10–H17	105.5909	108.1	H16–C10–C11–C13	55.7864	89.5
C10–H 17	1.0923	0.93	H16–C10–H17	107.2006	–	C11–C10–C12–N5	170.1915	–
C11–C 13	1.5325	1.5096	C10–C11–C13	112.272	112.36	C11–C10–C12–H20	51.6913	–
C11–H 18	1.0948	0.97	C10–C11–H18	109.8367	109.9	H16–C10–C12–N5	−66.6291	–
C11–H 19	1.0911	0.97	C10–C11–H19	110.808	109.9	H16–C10–C12–C14	56.9478	–
C12–C 14	1.5225	1.5215	C13–C11–H18	108.7247	109.9	H17–C10–C12–N5	48.2522	–
C12–H 20	1.0901	0.97	C13–C11–H19	108.204	109.9	H17–C10–C12–C14	171.8291	–
C13–H 21	1.1011	0.97	H18–C11–H19	106.8176	–	C10–C11–C13–H22	173.9905	–
C13–H 22	1.0997	0.97	N5–C12–C10	109.3509	108.91	H18–C11–C13–H22	52.2537	
			N5–C12–C14	112.0403	112.70	H19–C11–C13–N6	58.0127	–
			N5–C12–H20	108.5827	106.9	H19–C11–C13–H21	180.0053	–
			C10–C12–C14	110.205	110.92	N5–C12–C14–O1	−145.9414	–
			C10–C12–H20	108.8912	108.1	N5–C12–C14–O2	34.5676	–
			C14–C12–H20	107.6962	108.1	C10–C12–C14–O1	92.0592	–
			N6–C13–C11	110.1638	112.70	H20–C12–C14–O2	153.9112	–
			N6–C13–H21	110.821	–			
			N6–C13–H22	110.5304	–			
			C11–C13–H21	109.301	109.0			
			C11–C13–H22	108.974	109.9			
			H21–C13–H22	106.9761	–			
			O1–C14–O2	121.8545	125.77			
			O1–C14–C12	112.6682	115.67			
			O2–C14–C12	125.4753	–			
			N6–C15–N7	112.8266	–			
			N6–C15–N8	129.6759	122.15			
			N7–C15–N8	117.4975	118.36			

[a] Refer ref [16–19].

employing the 6-311G basis set.

2. Experimental details

The title compound, namely N-NLA was purchased from TCL chemicals. In the PERKIN ELMER spectrometer, the FT-IR spectrum of the compound is recorded in the range of 4000 cm^{-1}-400 cm^{-1}. The spectral resolution is ±2 cm^{-1}. UV–Vis spectrum was recorded in water solvent by using the Lambda-365 Perkin Elmer spectrophotometer range of 1100–190 nm as shown in Fig. 11. In Fig. 6, a 1H NMR spectrum of N-NLA was recorded using Dimethyl Sulphoxide (DMSO) as the solvent on a Bruker Avance 400 MHz FT-NMR spectrometer with TMS as the internal standard.

3. Computational details

The geometry for N-NLA is optimized using Becke's three parameter hybrid density function, B3LYP/6-311G, which includes DFT exchange correlation functional. The above calculations have been done using the Gaussian 09W software suite [11]. The simulated NMR (1H) chemical shifts were calculated with the GIAO method at same basis level. The TD-DFT method was used to calculate the theoretical UV–Vis parameters (wavelengths, oscillator strengths) at B3LYP/6-311G basis level. The MEP and HOMO-LUMO were computed at aforesaid basis level.

4. Results and discussions

4.1. Molecular geometry

Table 1 shows the optimized geometric parameters of the 6-311G basis set (bond lengths, bond angles, and dihedral angles) for the title compound. The molecule has 5N–H and 5N–C bond, 4 C–C bond, 7C–H bond, 2O–C bond and 2O–N bond and then one nitrogen atom (N) bond with nitrogen (N), one oxygen atom (O) bond with hydrogen (H) individually. Totally 28 atoms present in N-NLA. Therefore, 27 bonds among the atoms present in the compound C10–C12 exhibit the highest bond length of 1.5487 Å which state the weakest bond among the atoms and also O1–H25 exhibit the lowest bond length of 0.9783 Å which states that it is the strongest bond between the atoms. The bond length between O4–N9 gave a theoretical value 1.2754 Å which is equivalent to experimental value of 1.237 Å.There is a strong correlation between this experimental value and the theoretical value among the experimental and theoretical values [12–15]. The theoretical value of N7–C15 is 1.4283 Å [16–19] which is almost matched with the experimental value of 1.4718 Å. The minor difference is due to the gaseous state of molecule used in theoretical value. The experimental bond angle values of C–C–C,

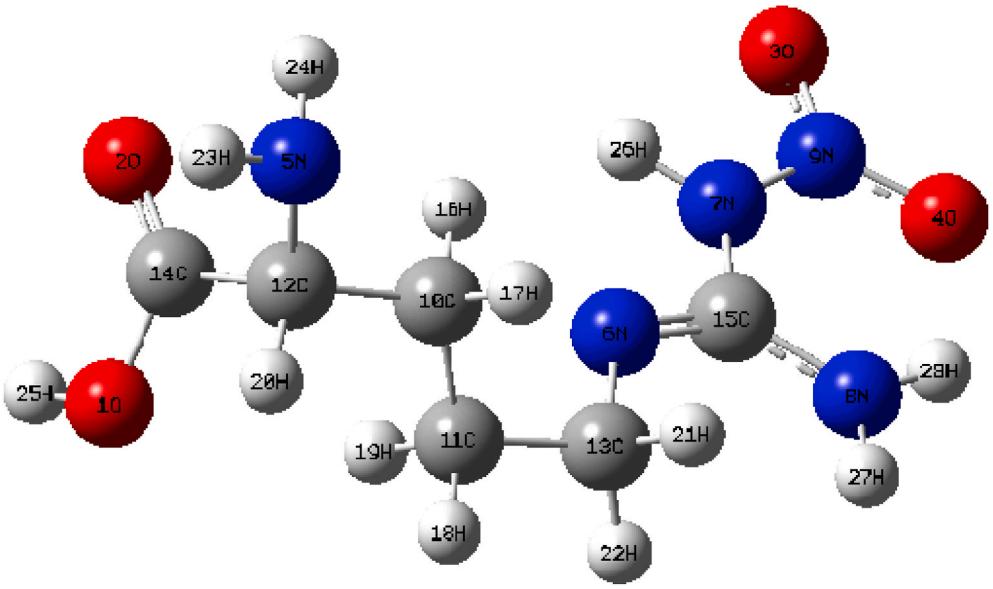

Fig. 1. Optimized structure of N_{ω}-nitro-L-Arginine.

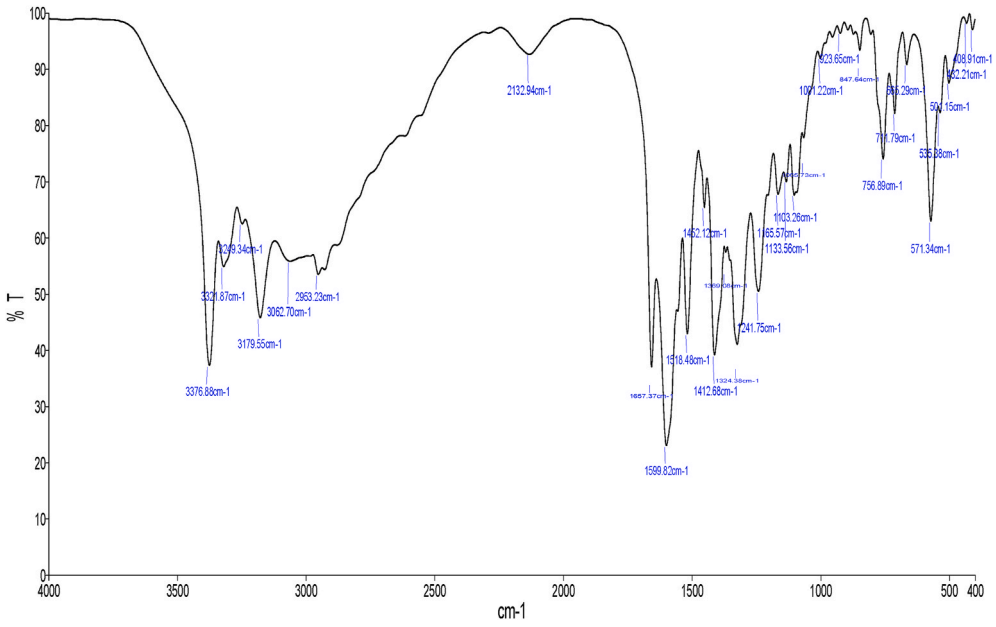

Fig. 2a. Experimental FTIR spectrum of N_{ω}-nitro-L-Arginin.

observed in the range of 108–115, show well correlation with calculated values. There may be a small difference between calculated bond angles and experimental values due to the fact that calculations pertain to the gas phase and experimental values pertain to the solid phase. The Optimized Structure of N_{ω}-Nitro-L-Arginine is shown in Fig. 1.

4.2. Spectral analysis

The N_{ω}-nitro-L-arginine compound contains 28 atoms. A normal coordinate analysis can provide a detailed description of vibrational modes. Based on a basis set 6-311G, theoretical frequencies can be observed using the DFT/B3LYP method. The experimental and theoretical FT-IR spectrum of the N-NLA is figured out in Fig. 2a and b and the observed and calculated fundamental modes of vibrations of N-NLA is collected in Table 2. In this paper, we propose assignment of vibrational frequencies based on calculated TED values. The stretching vibrations of NH_2 are naturally established in the range of 3300–3400 cm^{-1}. It has been determined that the IR band at 3377 cm^{-1} with weak intensity is NH_2 stretching vibrations. The theoretically computed value 3496 cm^{-1} is assigned for NH_2 stretching. The NH_2 out-of-plane bending has also seen at 712 cm^{-1}. In the current work NH_2 rocking mode is observed at 1242 cm^{-1} in FT-IR spectrum. The FT-IR band at 665 cm^{-1} and 432 cm^{-1} is designated as NH_2 wagging modes.

The C–H stretching vibrations are typically established in the range of 2600–3300 cm^{-1} [20–22]. In N-NLA compound, the stretching frequencies of C–H are observed at 3180 cm^{-1}. Theoretically C–C stretching vibrations were observed at 3089 cm^{-1}. The in-plane bending modes of C–H are observed between 1380 and 1465 cm^{-1}. Peaks at 1324 cm^{-1} are attributed to the aromatic C–H in-plane bending vibrations of N-NLA. The computed values by B3LYP/6-311G are in agreement with experimental values. The CH wagging mode appears at 848 cm^{-1}. For the title compound, the CH wagging modes are assigned at

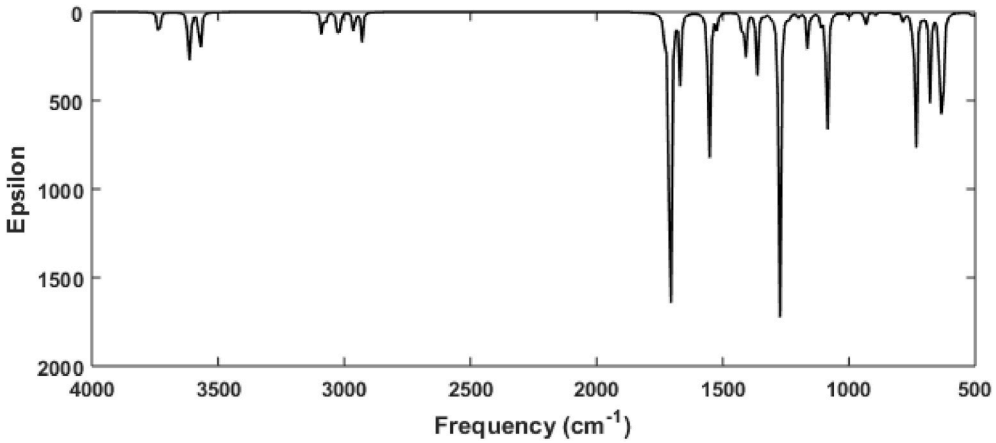

Fig. 2b. Theoretical FTIR spectrum of N_{ω}-nitro-L-Arginine.

Table 2
Vibrational assignments of wavenumbers for N_{ω}-Nitro-L-Arginine along with the theoretical wavenumbers at B3LYP/6-311G level.

S. No.	FT-IR Experimental wavenumbers (cm^{-1})	Theoretical wavenumbers (cm^{-1})	IR Intensity	Assignments
1	3377	3496	0.4642	νNH_2(97)
2	3180	3089	48.3665	νCH(95)
3	3062	3060	0.7568	$\nu_{as}CH_2$(86)
4	2953	2962	47.2484	νOH(92)
5	2132	2929	48.8448	$\nu_{as}CH_2$(86)
6	1657	1669	115.4591	νC = O (82)
7	1599	1554	324.6221	$\nu_{as}NO_2$(81)
8	1518.	1520	4.6919	δCH_2(76)
9	1452	1429	3.7528	δCH_2(76)
10	1413	1410	69.6515	CH_2 Twisting (74)
11	1369	1366	5.5019	$\nu_{as}NO_2$(75)
12	1324	1337	4.8401	δCH(83)
13	1242	1239	8.1525	NH_2 Rocking (71)
14	1165	1164	65.0807	ν_sC = N(89)
15	1133	1145	4.0350	CH_2 Rocking (73)
16	1103	1109	21.4513	ν_{as}C-O(82)
17	1065	1064	0.6152	CH_2 Wagging (64)
18	1001	999	13.8154	νC-C(78)
19	924	931	20.0023	γOH(65)
20	848	819	4.9533	CH_2 Wagging (64)
21	757	751	16.7043	CH_2 Rocking (73)
22	712	703	7.2945	γNH_2(61)
23	665	675	12.7384	NH_2 Wagging (58)
24	571	628	179.7281	δNO_2(69)
25	536	513	7.5483	NH_2 Rocking (71)
26	501	488	38.5458	NO_2 Wagging (69)
27	432	424	3.5719	NH_2 Wagging (70)
28	408	393	1.5201	δCN(74)

ν – stretching; δ – in plane bending; γ – out-of-plane bending.

819 cm^{-1} theoretically.

The N-NLA gives rise to CH_2 modes such as asymmetric stretching, in-plane bending, and twisting, wagging and rocking vibration. Due to aromatic C–H stretching vibrations, aromatic compounds usually exhibit multiple weak bands in the region of 3000–3100 cm-1 [23]. For aromatic compounds, the in-plane bending frequencies of C–H occur between 1000 and 1300 cm-1 and their out-of-plane vibrations appear between 750 and 1000 cm^{-1} [24,25]. The FT-IR bands are assigned at 3180, 3062 and 2132 cm^{-1} for CH_2 stretching vibrations in NNLA. The bands that seem at 1518 and 1452 cm^{-1} in FT-IR spectrum are due to CH_2 in plane bending vibration. The observed and calculated bending vibrations values are very much equal to each other. The twisting and wagging vibrations are identified at 1413, 1065 cm^{-1}. The rocking mode of the CH_2 seemed experimentally to be 1133, 757 cm^{-1}.

In the region around 3500 cm^{-1}, hydroxyl stretching vibrations are observed. O–H stretching vibration of N_{ω}-Nitro-L-Arginine is observed at 2953 cm^{-1} in FT-IR spectrum. In the present study, the calculated O–H stretching vibrational modes are obtained at 2962 cm^{-1} which coincides with the experimental wavenumber. Vibrations due to out-of-plane bending of O and H give rise to broadband in the range of 700–600 cm^{-1} [26]. In this present case, the O–H out of plane bending appeared at 924 cm^{-1}.

Generally, carbonyl group vibrations occur in the region 1850-1600 cm-1 [27]. In this study, the C═O stretching vibrations of N-NLA were observed at 1657 cm^{-1} in the FT-IR spectrum. Also, the C–O asymmetric stretching vibrations appeared at 1103 cm^{-1}.

Due to the asymmetric and symmetric stretching vibrations of the NO_2 group at 1625–1510 cm^{-1} and 1400 –1360 cm^{-1}, aromatic nitro compounds have strong absorptions [28]. The IR bands observed at 1599 cm^{-1} and 1369 cm^{-1} with strong intensity have been assigned to NO_2 asymmetric stretching vibrations. The in-plane deformation mode of the NO_2 group causes the aromatic nitro compounds to have a band of weak-to-medium intensity 590–500 cm^{-1} [29]. In this current work it is observed that the in plane bending vibrations at 571 cm^{-1}. The N–O in-plane bending mode is calculated at 628 cm^{-1} by theoretical method. The wagging mode of NO_2 identified at 501 cm^{-1}.

The C–N stretching absorption in occurs in the range 1382–1266 cm^{-1} for aromatic amines. In this compound, the C–N stretching vibration occurs at 1165 cm^{-1}. Consequently, the C–N in-plane bending vibration was found to be 408 cm^{-1}. These assignments are also maintained through the literature [30].

4.3. First hyperpolarizability

By using B3LYP with a 6-311G basis set based on the finite field approach, we calculated the first-order hyperpolarizability (β) of the molecular system. When an electric field is applied, the energy of the system is a function of the electric field. It is known that the first order of hyperpolarizability has the form of a third-rank tensor that can be described by a 3 × 3 × 3 matrix. The 27 components of the 3D matrix can be reduced to 10 components due to the Kleinman symmetry [31, 32].

The total static dipole moment μ, and the mean first hyper-

Table 4
Theoretical first heperpolarizability of N_ω-Nitro-L-Arginine using B3LYP/6-311G method.

Parameters	Values (amu)
β_{xxx}	439.5750
β_{xxy}	243.1933
β_{xyy}	−17.6668
β_{yyy}	−138.9299
β_{xxz}	47.3368
β_{yyz}	−5.3651
β_{xzz}	−47.1535
β_{yzz}	−0.8440
β_{zzz}	−165.9066
β	**3.5250×10^{-30} esu**

polarizability (β) using the x, y, z components, they are defined as

$$\mu = \left(\mu_x^2 + \mu_y^2 + \mu_z^2\right)^{1/2} \tag{1}$$

$$\text{where } \beta = \left(\beta_x^2 + \beta_y^2 + \beta_z^2\right)^{1/2}$$
$$\beta_x = \beta_{xxx} + \beta_{xyy} + \beta_{xzz}$$
$$\beta_y = \beta_{yyy} + \beta_{xxy} + \beta_{yzz} \tag{2}$$
$$\beta_z = \beta_{zzz} + \beta_{xxz} + \beta_{yyz}$$

The components of first order hyperpolarizability of N_ω-Nitro-L-Arginine are reported in Table 4. The first order hyperpolarizability of N-NLA is 3.5250×10^{-30} esu which is 9 times greater than urea ($\beta = 0.3727 \times 10^{-30}$ esu) which shows that N-NLA has NLO property.

4.4. Analysis of Fukui indices

The study of the population of electrons around the atoms in a molecule is also useful to study the stability of the molecule. Complete pictures of the electronic charge density of the molecule are viewed through Mullikan population analysis and the technique given by Yang and Mortier [33–35]. In this study, the condensed Fukui function f_k has been calculated at 6-311G level of theory. For a system of N electrons, independent calculations have been made corresponding to a N - 1; N and N + 1 electron system. The Mullikan population analysis produces (N – 1), (N) and (N + 1) for all atoms k: In a finite difference approximation, the f_k values are calculated by

$$f_k^n = q_k(N+1) - q_k(N) \quad \text{for nucleophilic attack} \tag{3}$$

$$f_k^e = q_k(N) - q_k(N-1) \quad \text{for electrophilic attack and} \tag{4}$$

$$f_k^r = \frac{1}{2}q_k(N+1) - q_k(N-1) \quad \text{for radical attack} \tag{5}$$

We optimize N_ω-Nitro-L-Arginine at three different charge states, i.e., neutral, positively charged, and negatively charged. The Fukui function values are shown in Table 7 and indicate a significant difference in charge between the atoms. The charge distributions show that N8 is the preferred active site for reaction with nucleophilic species, and C15 with electrophilic species. The favoured active site for the reaction with radical attack is N9. The calculated values of the Fukui functions are shown in Table 7 and Fig. 3.

The local softness, S^+ and S^- for an atom can be expressed as the product of the Fukui function, f_k^e, and f_k^n the global softness, S, as follows:

$$S^+ = f_k^n S \tag{6}$$

$$S^- = f_k^e S \tag{7}$$

Local softness represents information similar to that derived from the Fukui function, as well as information about the molecular softness, which is associated with a reaction partner's global reactivity. Calculated values of S^+ and $S^-$are presented in Table 7.

4.5. Influence of electric fields on HOMO–LUMO analysis

The energy gap of the N-NLA has been calculated in Table 3 at B3LYP/6-311G level for electric fields such as 0, 0.5, 0.1, 0.15, and 0.25 VA^{-1} as well as indicating that the energy gap reflects the chemical activity of the molecule. As the electric field is increased the HOMO-LUMO gap reduces widely from 4.7804 eV to 0.3234 eV. the energy gap of N_ω-nitro-L-arginine is decreased, As the electric field is increased which

Table 7
Condensed Fukui functions for calculated N_ω-Nitro-L-Arginine at B3LYP/6-311G method.

ATOMS	q_kN	q_kN_{-1}	q_kN_{+1}	f_k^e	f_k^n	f_k^r	S^+	S^-
O1	−0.5589	0.0025	−0.0000	−0.5614	0.5589	−0.0012	−0.2349	0.2338
O2	−0.3756	−0.0009	0.0000	−0.3747	0.3756	0.0005	−0.1567	0.1571
O3	−0.2712	−0.0027	0.2808	−0.2684	0.5521	0.1418	−0.1123	0.2309
O4	−0.3179	0.0065	0.2302	−0.3244	0.5482	0.1118	−0.1357	0.2293
N5	−0.6703	0.4875	−0.0000	−1.1579	0.6703	−0.2437	−0.4844	0.2804
N6	−0.3659	0.3378	0.0207	−0.7038	0.3866	−0.1585	−0.2944	0.1617
N7	−0.5029	0.0444	0.0497	−0.5473	0.5527	0.0026	−0.2289	0.2312
N8	−0.8186	0.0947	0.0014	−0.9133	**0.8200**	−0.0466	−0.3821	0.3430
N9	0.3319	−0.0064	0.4153	0.3383	0.0834	**0.2108**	0.14154	0.0349
C10	−0.3184	0.0591	0.0001	−0.3775	0.3186	−0.0294	−0.1579	0.1332
C11	−0.3176	0.0282	0.0001	−0.3458	0.3177	−0.0140	−0.1447	0.1329
C12	−0.1430	−0.0218	0.0001	−0.1211	0.1430	0.0109	−0.0506	0.0598
C13	−0.3013	−0.0179	−0.0022	−0.2834	0.2990	0.0078	−0.1185	0.1251
C14	0.4987	0.0069	−0.0000	0.4918	−0.4987	−0.0034	0.2057	−0.2086
C15	0.7631	−0.0476	0.0019	**0.8108**	−0.7612	0.0248	0.3392	−0.3184
H16	0.1918	0.0012	−0.0002	0.1905	−0.1920	−0.0007	0.0797	−0.0803
H17	0.1919	−0.0020	0.00001	0.1940	−0.1919	0.0010	0.0811	−0.0803
H18	0.1673	−0.0013	−0.0007	0.1687	−0.1674	0.0006	0.0705	−0.0700
H19	0.1898	−0.0020	0.0006	0.1919	−0.1897	0.0010	0.0803	−0.0794
H20	0.2053	0.0124	0.000016	0.1929	−0.2053	−0.0062	0.0807	−0.0859
H21	0.1723	0.0071	0.0013	0.1651	−0.1710	−0.0029	0.0690	−0.0715
H22	0.1780	0.0620	0.0018	0.1160	−0.1762	−0.0301	0.0485	−0.0737
H23	0.2894	−0.0197	0.0000	0.3092	−0.2894	0.0098	0.1293	−0.1211
H24	0.2965	−0.0187	0.0002	0.3152	−0.2965	0.0093	0.1319	−0.1240
H25	0.3824	0.0010	−0.0001	0.3814	−0.3824	−0.0005	0.1595	−0.1600
H26	0.3809	−0.0027	0.0021	0.3836	−0.3788	0.0024	0.1605	−0.1584
H27	0.3517	−0.0038	−0.0005	0.3556	−0.3522	0.0016	0.1487	−0.1473
H28	0.3703	−0.0036	−0.0028	0.3739	−0.3731	0.0003	0.1564	−0.1561

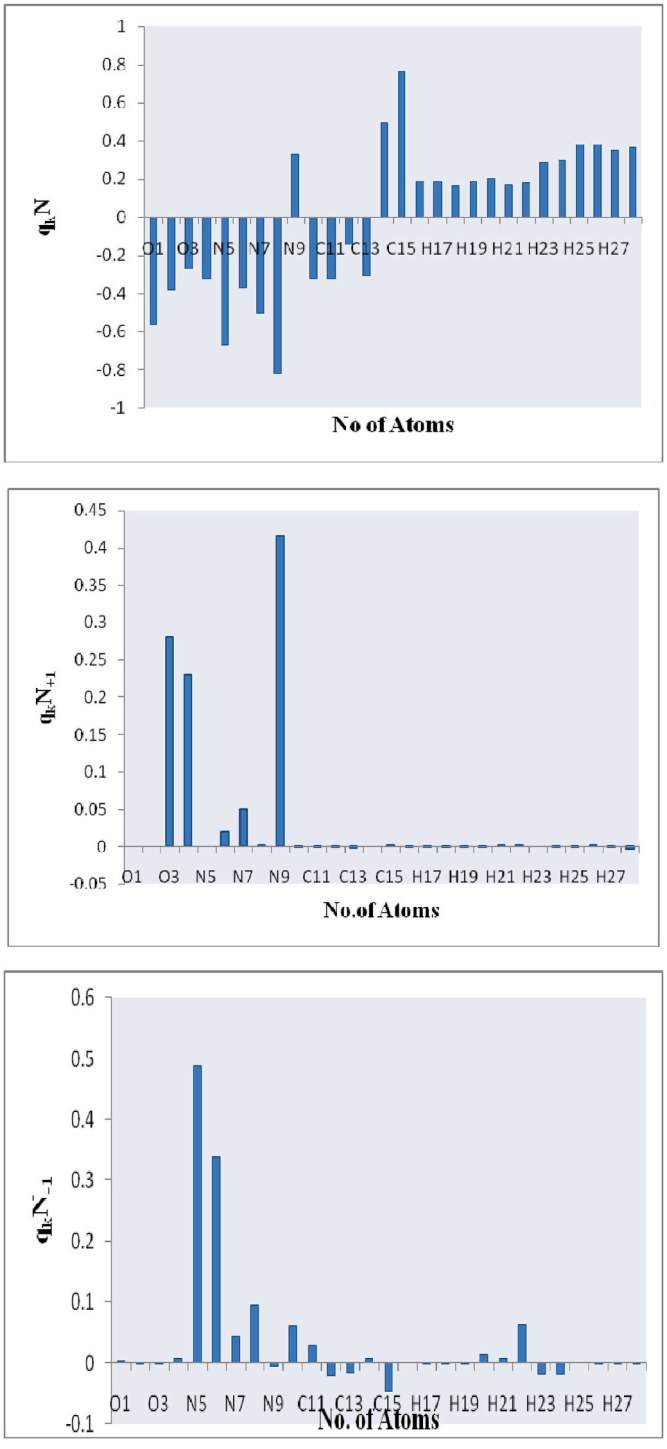

Fig. 3. Fuki indices of N_ω-nitro-L-Arginine.

showing that the conductivity has also increased.

4.6. Transport properties

The wave function analysis indicates that the electron absorption correlates with the transition from the ground state to the first excited state mainly due to one-electron excitations from the HOMO to the LUMO. HLG stands for HOMO-LUMO gap, which is the potential energy difference between HOMO and LUMO [36,37]. The HLG is one of the key factors determining the transport properties of the molecule [38]. The possibility of good conduction through the molecule increases with large decreases in the energy gap. The conductivity increases as the HOMO-LUMO gap decreases [39]. At the B3LYP/6-311G level the HOMO-LUMO energy gap of N-NLA is calculated. The orbital distribution of HOMO-LUMO levels of the N-NLA is shown in Fig. 4. HOMO spreads mainly on nitrogen and hydrogen of the NH_2 group and LUMO spreads mainly on nitrogen and oxygen which is NO_2 for zero electric field. In N-NLA, the calculated energy value of HOMO is −8.2105eV and the energy value of LUMO is −3.4301eV. Therefore, the HOMO LUMO energy gap is 4.7804, explaining the charge transfer interactions taking place inside the molecule.

Table 3
The HOMO-LUMO gap (HLG) values (in eV) of N_ω-Nitro-L-Arginine using B3LYP/6-311G method.

Electric field in VÅ^{-1}	N_ω-Nitro-L-Arginine		
	E_{HOMO}	E_{LUMO}	HLG
0	−8.2105	−3.4301	4.7804
0.05	−7.9346	−4.3854	3.5491
0.1	−6.9731	−5.3546	1.6185
0.15	−6.3211	−6.0089	0.3122
0.2	−6.0256	−5.0431	0.9825
0.25	−5.0976	−4.7742	0.3234

4.7. Global reactivity descriptors

Compounds are calculated based on their hardness, softness, chemical potential, and electron negativity in order to understand the global nature of their stability and their reactivity. The chemical hardness (η) and chemical potential (μ) are calculated using Koopmans' theorem [40].

$$\eta = \frac{I - A}{2} \tag{8}$$

$$S = \frac{1}{\eta} \tag{9}$$

$$\mu = \frac{-(I + A)}{2} \tag{10}$$

$$\chi = \frac{(I + A)}{2} \tag{11}$$

where I and A are the ionization potential and electron affinity of the compounds, respectively. Higher ionization energy results in chemical stability and inertness, while lower ionization energy results in high reactivity of the molecule. HOMO energy directly correlates with ionization potential (IP), while LUMO energy directly correlates with electron affinity (EA). In this study, the molecules N_ω-Nitro- L-Arginine the Ionization value is high for zero electric field and the electric field is increased the value of I is also decreases. Also while adding the solvent; there are minor changes in ionization potential. The HOMO–LUMO energy gaps of all the electric fields are shown in Fig. 4 and also tabulated in Table 5. Also DOS of N_ω-Nitro-L-Arginine for the zero and various applied fields are shown in Fig. 5.

The chemical hardness of an atom, ion, or molecule is determined by its resistance to its electron cloud being deformed or polarized under a perturbation in the chemical reaction. In N_ω-Nitro- L-Arginine has, the hardness value of the title compound in the gas phase is 2.3902 eV and the softness is 0.4183 eV (Table 5). In all the polar and non-polar solvents, the chemical hardness is at its minimum value, which shows that the chemical reactivity is enhanced in all the solvents.

Chemical potential (μ) describes the tendency of electrons to escape from an equilibrium system and its values are calculated by equation (5) and presented in Tables 5 and 6 for different electric fields and different solvents. The higher the electronic chemical potential, the less stable or more reactive the compound is. This table indicates that water solvent is

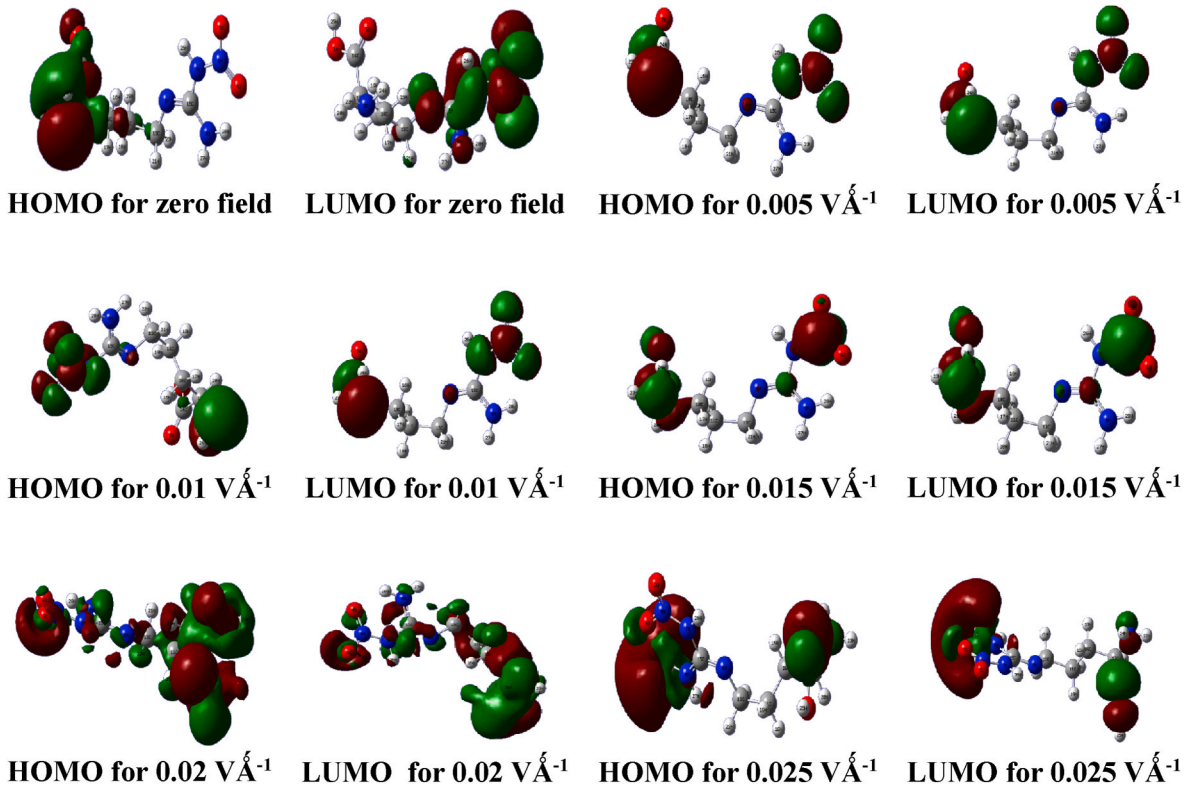

Fig. 4. Isosurface representation of molecular orbitals for N_{ω}–Nitro-L-Arginine for the zero and various applied fields.

Table 5
The theoretical HOMO energy, LUMO energy, Energy gap (Eg) and Ionization potential (IP), Electron affinity (EA), Hardness (σ), Softness (s), Chemical potential (μ), Electronegativity (χ), Electrophilicity index (ω), Nucleofugality (ΔEn) and Electrofugality (ΔEe) of N_{ω}-Nitro-L-Arginine using B3LYP/6-311G method.

Parameters	Electric field in VÅ^{-1}					
	0	0.05	0.1	0.15	0.2	0.25
HOMO energy E_H	−8.2105	−7.9346	−6.9731	−6.3211	−6.0256	−5.0976
LUMO energy E_L	−3.4301	−4.3854	−5.3546	−6.0089	−5.0431	−4.7742
Energy Gap Eg	4.7804	3.5491	1.6185	0.3122	0.9825	0.3234
Ionization potential IP	8.2106	7.9346	6.9732	6.3212	6.0257	5.0977
Electron affinity EA	3.43012	4.3854	5.3546	6.0089	5.0431	4.7742
Hardness Ƞ	2.3902	1.7746	0.8093	0.1561	0.4913	0.1617
Softness S	0.4183	0.5635	1.2357	6.4056	2.0354	6.1836
Chemical potential μ	−5.8204	−6.1600	−6.1639	−6.1650	−5.5343	−4.9359
Electronegativity χ	5.8204	6.1600	6.1639	6.1650	5.5343	4.9359
Electrophilicity index ω	7.0865	10.6915	23.4748	121.7340	31.1727	75.3278
Nucleofugality ΔE_n	2.4612	5.4188	17.7150	115.647	25.8839	70.4730
Electrofugality ΔE_e	14.10192	17.7388	30.0433	127.977	36.9527	80.3445

less stable among various solvents, including water, aniline, DMSO, Ethanol, Chloroform, and Thiophene.

The electrophilicity index (ω) is used to quantify the energy lowering due to maximal electron flow from donor to acceptor. The electrophilicity index (ω) is defined as

$$\omega = \frac{\mu^2}{2\eta} \tag{12}$$

The effectiveness of this new reactivity level has been shown in recognizing the harmfulness of different contaminants in terms of their reactivity and site selectivity. [Selvam, L. Antony et al., 2020; Farmer, Edward E. et al., 2007; Du, Y. L. et al., 2009]. The N_{ω}-Nitro- L-Arginine has low electrophilicity is presented in Table 5. From this table, it is evident that the solvent and electric field substituents are increasing the electrophilicity index.

The maximum amount of electronic charging that the electrophile system can accept is provided by Ref. [41].

$$\Delta N = \frac{\chi_{Fe} - \chi_{Inh}}{2(\eta_{Fe} + \eta_{Inh})} \tag{13}$$

where χ_{Fe} and χ_{Inh} represent the absolute electronegativity of iron and inhibitor molecule respectively. η_{Fe} and η_{Inh} represent the absolute hardness of iron and the inhibitor molecule respectively. Theoretical value of $\chi_{Fe} = 6.38775$ eV and $\eta_{Fe} = 0$ for the computation of number of transferred electrons. Condensed Fukui function is the best method to quantify the local selectivity of corrosion inhibitors. The difference in electronegativity determines electron transfer, and the sum of the hardness parameters acts as a resistance.

An electronic back-donation is shown in the following equation

$$\Delta E_{back-donation} = -\frac{\eta}{4} \tag{14}$$

The two new reactivity indices to quantify the nucleophilic and electrophilic capabilities of leaving group are nucleofugality (ΔEn) and

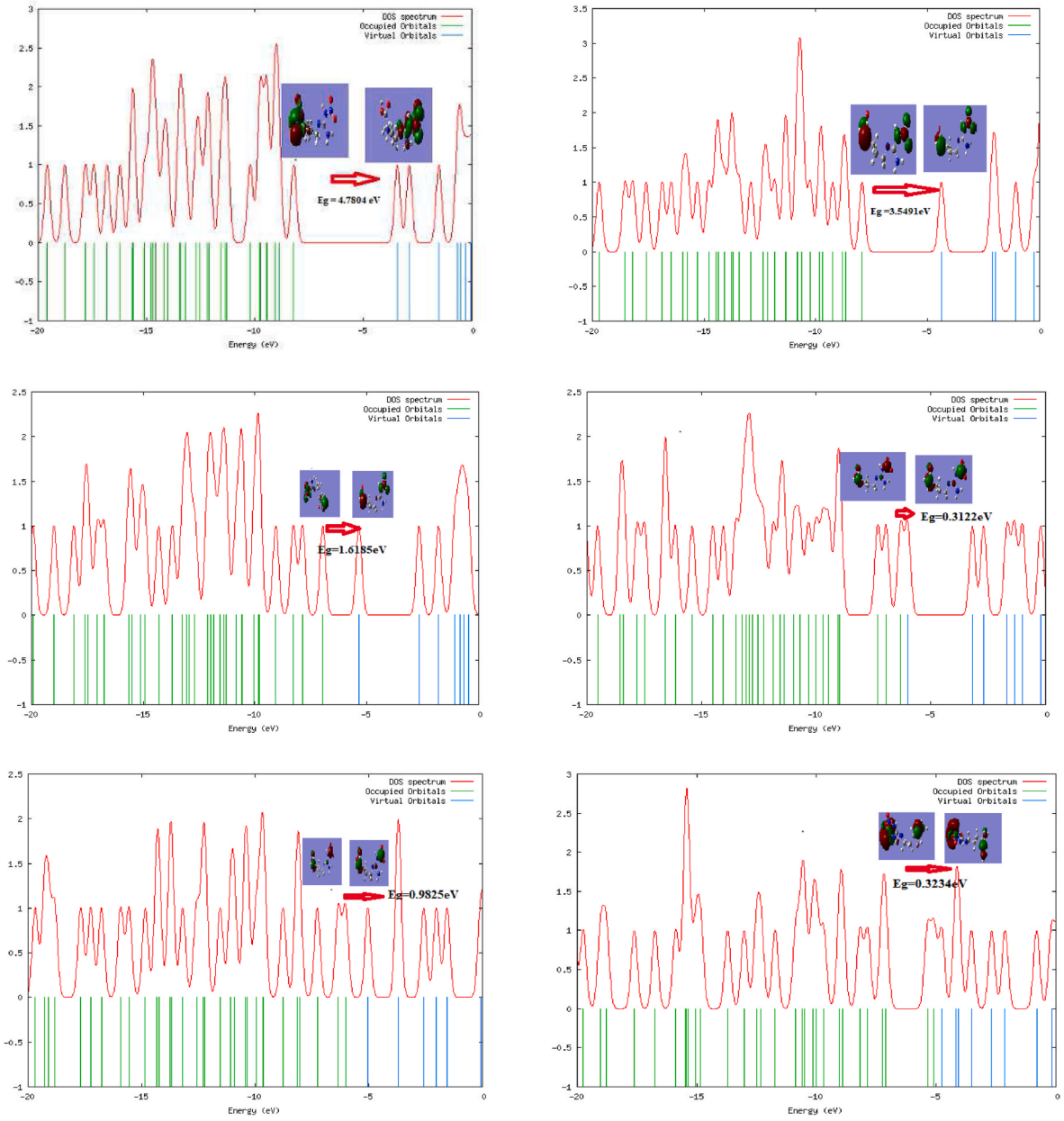

Fig. 5. DOS of N_{ω}–Nitro-L-Arginine for the zero and various applied fields.

electrofugality (ΔEe) and they are defined as follows

$$\Delta E_n| = EA + \omega = \frac{(\mu + \eta)^2}{2\eta} \tag{15}$$

$$\Delta E_e = IP + \omega = \frac{(\mu - \eta)^2}{2\eta} \tag{16}$$

As shown in Table 6, the values of nucleofugality (ΔEn) and electrofugality (ΔEe) are almost identical for all the solvents, as well as for a 0.015 VA*1 electric field, which gives the maximum values of ΔEn and ΔEe.

4.8. Electrostatic potential analysis

MEP is correlated to electronic density and can be used to determine the sites for electrophilic and nucleophilic reactions, as well as hydrogen bonding interactions [42–44]. At a point around a molecule, the molecular electrostatic potential (MEP) gives an indication of the net electrostatic effect generated at that point from the nuclei and electrons in the molecule, and is correlated with the dipole moments, electronegative properties, and chemical activity of molecules [45]. It provides a visual method to understand the relative polarity of the molecule. Electrostatic potential for zero and different applied electric fields are shown in Fig. 6. The various values of the electrostatic potential at the surface are represented by various colours. It is possible to see the slightly electron deficient region (light blue) over the N atoms. The neutral region is found at amino group. When the electric field is applied the positive ESP is identified by the blue region in the amino group, also the red region represents negative ESP which is established over NO_2 atoms. This progress is almost remaining the same when the field increased to 0.025 $VÅ^{-1}$.

4.9. Solvent effect in UV-VIS analysis

The high absorption (λ_{max}) of NNLA is detected by the TD-DFT/B3LYP method using 6-311G. The calculated maxima of λ_{max}

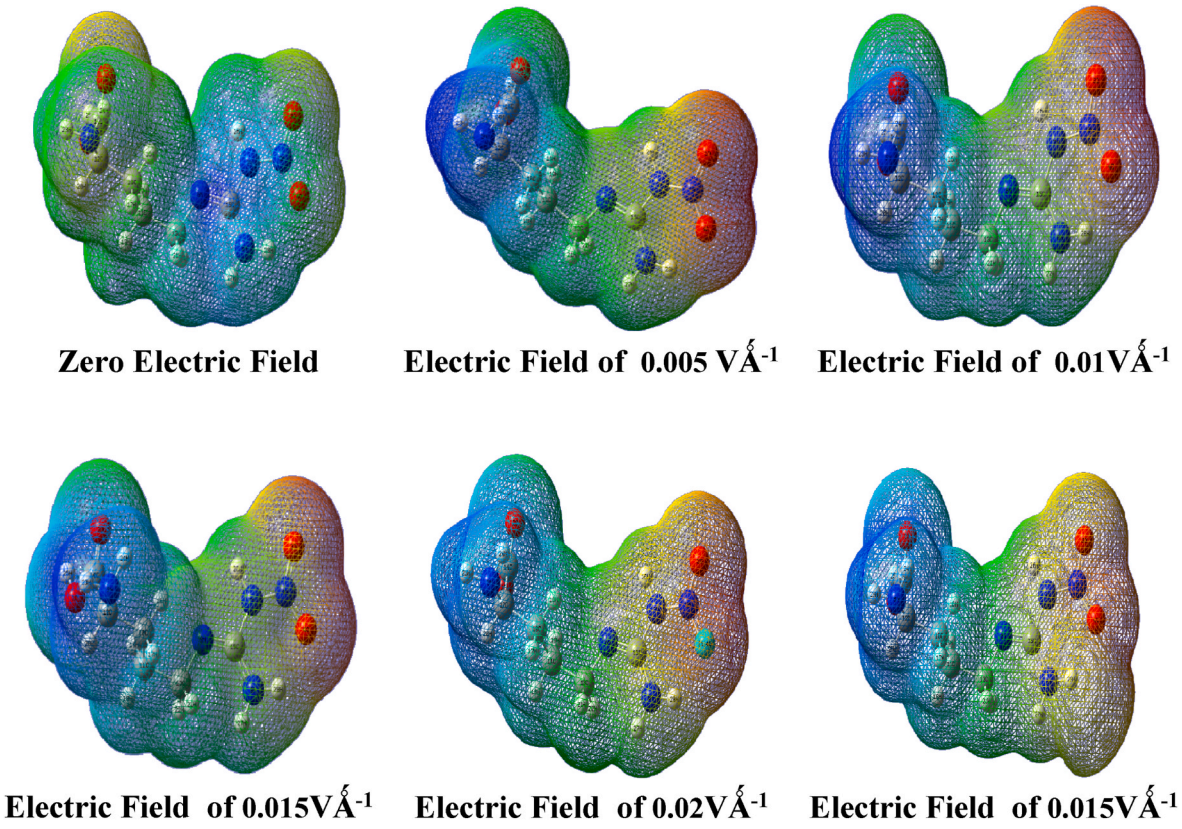

Fig. 6. Isosurface representation of electrostatic potentials of N–Nitro-L-Arginine for the zero and various applied field.

Table 6
The theoretical HOMO energy, LUMO energy, Energy gap (Eg) and Ionization potential (IP), Electron affinity (EA), Hardness (σ), Softness (s), Chemical potential (μ), Electronegativity (χ), Electrophilicity index (ω), Nucleofugality (ΔEn) and Electrofugality (ΔEe) of $N_ω$-Nitro-L-Arginine with solvents using B3LYP/6-311G method.

Parameters	Values (eV)							
	Water	DMSO	Aniline	Ethanol	CCL_4	Thiophene	Chloroform	Cyclo Hexane
HOMO energy E_H	−8.2098	−8.2099	−8.2107	−8.2100	−8.2111	−8.2107	−8.2109	−8.2110
LUMO energy E_L	−3.4445	−3.4443	−3.4416	−3.4438	−3.4364	−3.4418	−3.4403	−3.4357
Energy Gap Eg	4.7652	4.7656	4.7691	4.7662	4.7747	4.7688	4.7706	4.7753
Ionization potential IP	8.2098	8.2099	8.2108	8.2101	8.2112	8.2107	8.2110	8.2111
Electron affinity EA	3.4445	3.4443	3.4416	3.4438	3.4364	3.4418	3.4403	3.4357
Hardness Ƞ	2.3826	2.3828	2.3846	2.3831	2.3874	2.3844	2.3853	2.3877
Softness S	0.4197	0.4196	0.4193	0.4196	0.4188	0.4193	0.4192	0.4188
Chemical potential μ	−5.8272	−5.8271	−5.8261	−5.8269	−5.8237	−5.8262	−5.8256	−5.8234
Electronegativity χ	5.8272	5.8271	5.8261	5.8269	5.8237	5.8262	5.8256	5.8234
Electrophilicity index ω	7.1258	7.1251	7.1174	7.1238	7.1033	7.1180	7.1138	7.1014
Nucleofugality $ΔE_n$	2.4899	2.4894	2.4836	2.4884	2.4732	2.4840	2.4809	2.4719
Electrofugality $ΔE_e$	14.14431	14.1436s	14.1359	14.14242	14.1207	14.13659	14.1322	14.1187

Table 8
Theoretical absorption wavelength λ (nm), excitation energies E (eV) and oscillator strengths (f) of $N_ω$-Nitro-L-Arginine using TD-DFT/B3LYP/6–311G method in gas and solvents.

Parameters	Gas Phase	Aniline	DMSO	Ethanol	Water	Chloroform	Thiophene
Wavelength (λ)	331.21	353.53	357.41	356.37	357.32	350.79	353.11
Excitation energies (E)	3.7433	3.5071	3.4689	3.4790	3.4698	3.5345	3.5112
Oscillator strengths (f)	0.0876	0.1021	0.0964	0.0949	0.0937	0.0976	0.0970
LHE	0.1826	0.2095	0.19906	0.1962	0.1940	0.2012	0.2001
Transition with contribution	H-1→L (97.09%)	H-1→L (91.17%)	H-1→L (75.89%)	H-1→L (80.75%)	H-1→L (72.46%)	H-1→L (88.55%)	H-1→L (88.87%)

absorption, oscillator strength, excitation potential, and transition with contributions are reported in Table 8. This high absorption is caused by the electron switching from HOMO-1 to LUMO [46,47]. Absorption maxima found at 214.35, 268.10 nm experimentally. The theoretical & experimental UV–Vis spectrums of $N_ω$ Nitro-L-Arginine are shown in Figs. 7–9 also the theoretical UV-VIS spectrum of various solvents are figured out in 10 (see Fig. 10).

All of these outputs from the NNLA show a high absorption peak between 330 and 360 nm of the S0 → S1 transition, which provides significant red shifted absorption comparatively. The calculated

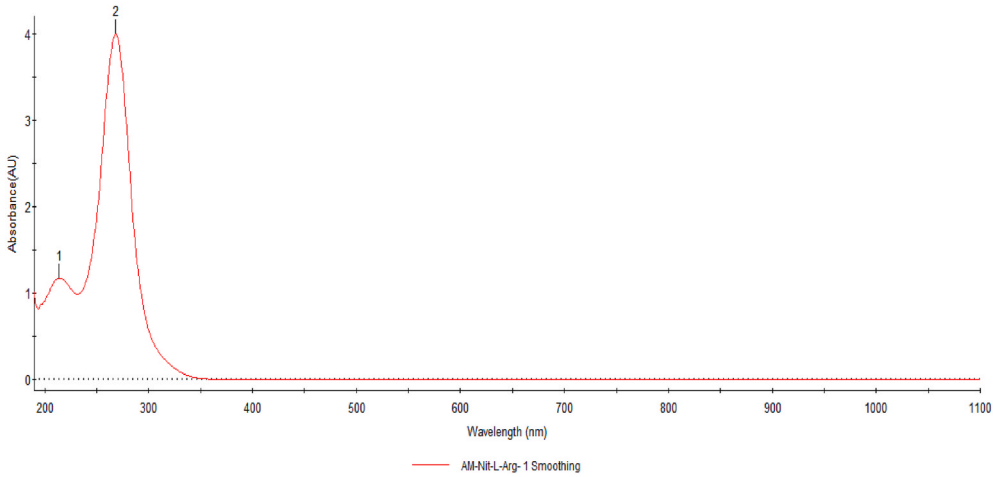

Fig. 7. Experimental UV-VIS Absorption spectrum of N_{ω}-Nitro-L-Arginine.

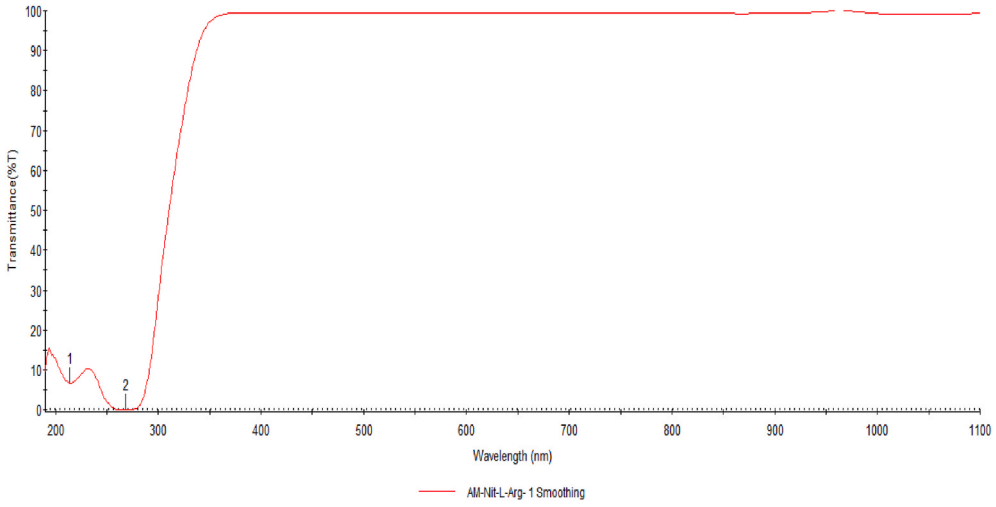

Fig. 8. Experimental UV-VIS Transmission spectrum of N_{ω}– Nitro- L-Arginine.

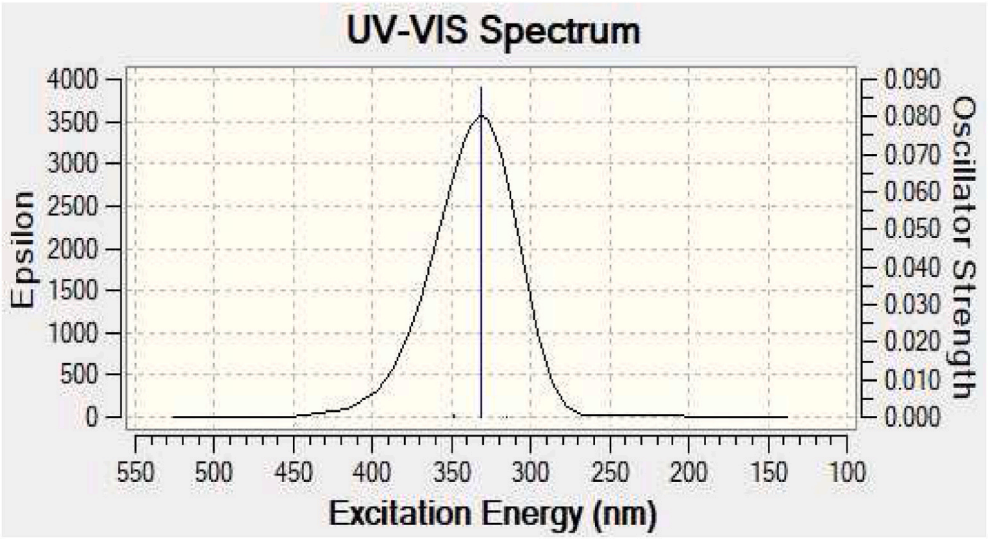

Fig. 9. Theoretical UV-VIS spectrum of N_{ω}-Nitro-L-Arginine.

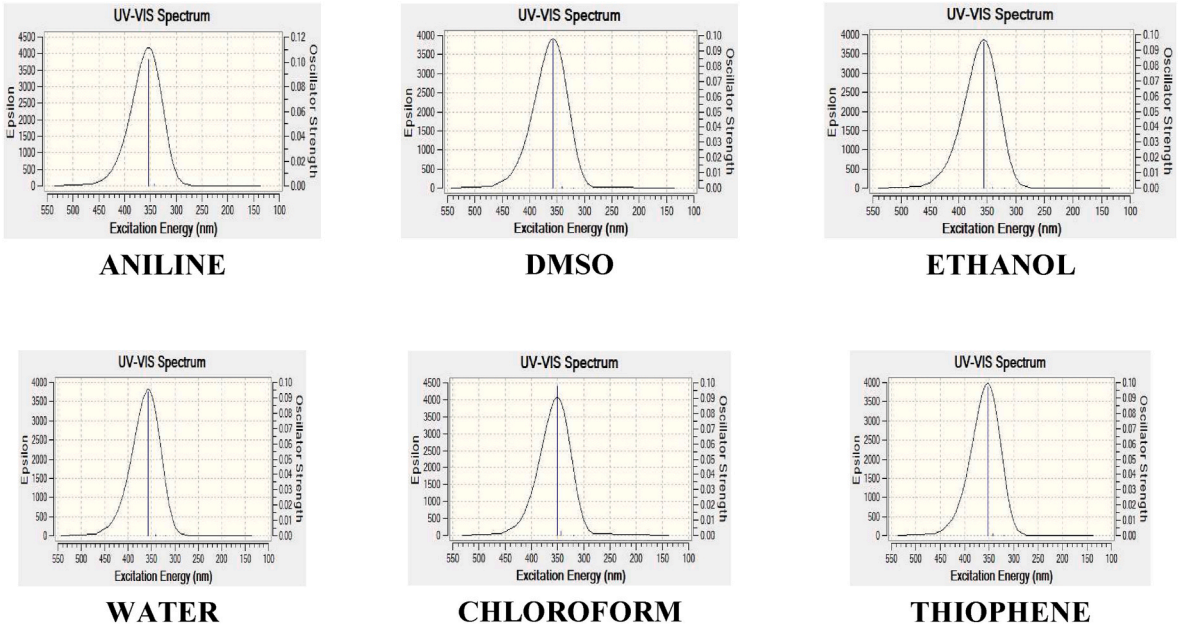

Fig. 10. Theoretical UV-VIS spectrum for various solvent of N_{ω}-Nitro-L-Arginine.

Table 9
The calculated ^{1}H NMR isotropic chemical shifts (all values in ppm) for N_{ω}-Nitro-L-Arginine using GIAO method.

Atoms	Experimental Chemial shift	Theoretical	
		Chemical shift	Chemical shielding
H16	2.087	1.8508	30.7468
H17	1.680	1.5619	31.0357
H18	1.603	1.5081	31.0895
H19	1.234	1.525	31.0726
H20	3.227	3.2644	29.3332
H21	2.509	2.8757	29.7219
H22	3.164	3.1462	29.4514
H23	1.151	1.0075	31.5901
H24	–	0.9926	31.6050
H25	–	6.5553	26.0423
H26	8.652	9.1008	23.4968
H27	3.416	3.7726	28.8250
H28	–	6.4506	26.1470

maximum absorption values were predicted at 331.21 nm and 357.41 nm in the gas phase and the polar and non-polar solvents, respectively. The highest absorption wavelength in the calculated spectrum corresponds to the electronic transition from HOMO -1 to LUMO in gases with a contribution of 68% and from HOMO-1 to LUMO in solvents with a contribution of 85%. The highest peak at 357.41 nm was achieved in DMSO. These solvent components improve the oscillator strength to a higher level. Therefore this NNLA can be used for DSSC applications.

4.10. NMR analysis

Isotropic chemical shifts are generally used to identify reactive organic and ionic species. To accurately predict the magnetic properties of molecules, exact molecular geometries must be predicted. So, complete geometry optimization of NNLA are performed using B3LYP/6-311G method in Gas, DMSO solvent. Then ^{1}H chemical shift calculations of the title compound were made using same method and basis set by GIAO and the values of chemical shift is reported in Table 9.

The experimental values of ethylene group ^{1}H NMR, lie between 1.234 and 2.087 ppm correspondingly the theoretical values lie between 1.5081 and 1.8508 ppm. From this, it is observed that there is a quiet agreement between experimental and theoretical values. The ^{1}H experimental and theoretical NMR spectrum is shown in Fig. 11a and b..

4.11. Corrosion inhibitor efficiency

A corrosion inhibitor is best effective and economical ways to shield the exterior surface of metal (ferrous and copper) commonly used in the industry for protecting the environment. Generally, corrosion inhibitors contained nitrogen, sulfur, oxygen and phosphorous, as well as aromatic rings. They are generally responsible for corrosion protection [48]. By adsorbing on the metal surface, these compounds form a protective layer that prevents corrosion causing elements from coming in interaction through the metal surface [49,50].

Though, most of these compounds being artificial chemicals and are expensive and also harmful to both human and the green environment. Therefore, it should be replaced with non-toxic and eco-friendly compounds [51]. The study of reaction mechanisms has generally relied on quantum chemical calculations. Studies of corrosion inhibition mechanisms have proven that they are extremely effective. The amino acids belong to organic compounds that are non-toxic, highly soluble in water, decompose easily, and are affordable to produce at high purity [52].

It was noted that the existence of heteroatoms (N, S, P and O) in the organic molecule improves their performance as a ferrous corrosion inhibitor. There is a single electron pair in the N and O atoms, which contributes to the formation of chemical bonds on the surface of metal atoms. The N-NLA contains both the nitrogen and oxygen atoms in its structure. This allows N_{ω}-Nitro-L-Arginine to act as a corrosion inhibitor.

Based on the calculated values of global reactivity descriptor, the effectiveness of title compound can be investigated. The hardness (η) and the softness (S) of the cell measure the stability and chemical reactivity of a molecule. Conversely, a molecule with a high global softness value will adsorb and react more readily with the metal surface. Molecule with lower value of η (and higher value of σ) shows higher corrosion inhibition efficiency [53].

In the current study, the value of N-NLA 3 has the lowest value of η as given in Table 10. It can be interpreted that N-NLA 3 has a very high between the four molecules under consideration. The number of transferred electron (ΔN) from the inhibitor molecule to the surface Fe atoms was calculated using equation (15). Depends upon the polarity (positive or negative) of ΔN, electron transfer takes place from the inhibitor molecule to the Fe surface and vice-versa. From Table 10, it confirms

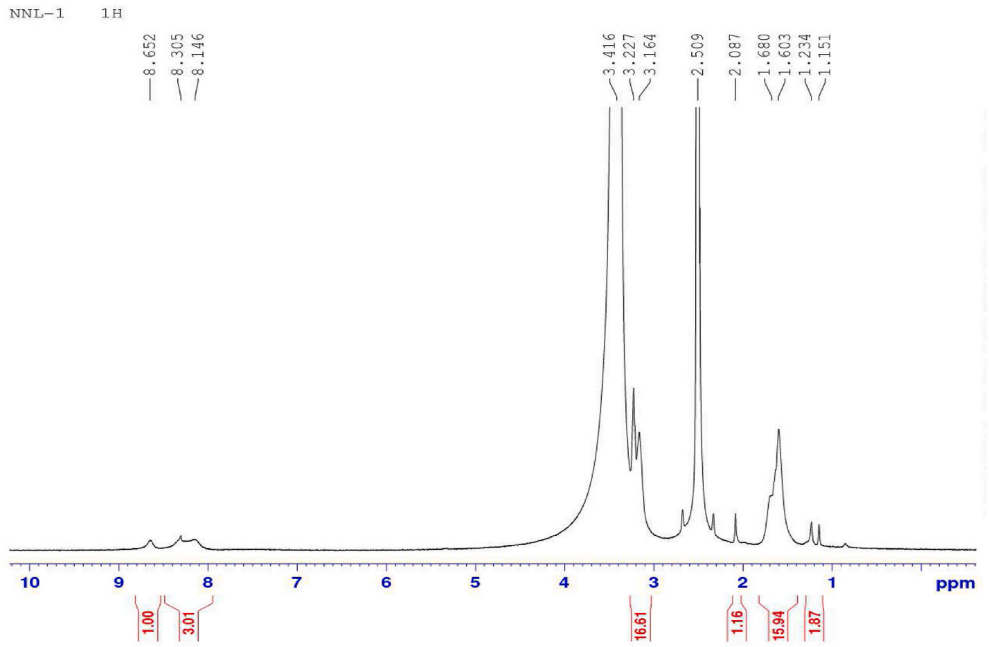

Fig. 11a. Experimental ^{1}H NMR Spectra of N_{ω}-Nitro-L-Arginine in DMSO solvent.

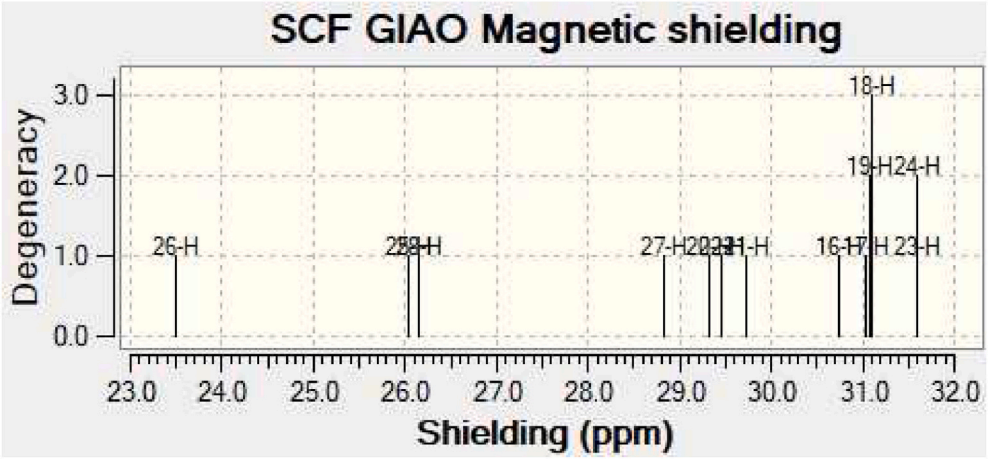

Fig. 11b. Theoretical ^{1}H NMR Spectra of N_{ω}-Nitro-L-Arginine in DMSO solvent.

Table 10
Calculated values of E_{HOMO}, E_{LUMO}, Electronegativity (χ) and ΔN values for N_{ω}-Nitro-L-Arginine with donor variations using DFT/B3LYP/6-311G method.

Systems	E_{HOMO} (eV)	E_{LUMO} (eV)	Energy gap (Eg) (eV)	χ (eV)	η (eV)	ΔN	$\Delta E_{back\text{-}donation}$
N-NLA	−8.2105	−4.1021	4.7804	5.8203	2.3902	−0.0974	0.7275
N-NLA 1 Donor: Pyrole; Acceptor: Cyanoacrylic	−7.7474	−5.0190	2.7284	6.3832	1.3641	0.00164	−0.34105
N-NLA 2 Donor: Furan; Acceptor: Cyanoacrylic	−7.112904	−5.08748	2.02542	6.1001939	1.0127	0.1419	−0.2531
N-NLA 3 Donor: Thiophene; Acceptor: Cyanoacrylic	**−6.7079**	−5.0161	**1.6918**	5.8620	0.8451	**0.3110**	**−0.2112**
N-NLA 4 Donor: Azulene; Acceptor: Cyanoacrylic	**−7.7405**	−5.0201	**2.7204**	6.3803	1.3602	**0.0027**	**−0.34005**

that all the ΔN values are positive, thus indicating adsorption through electron donation by the inhibitor molecules. The electron back donation (ΔEback-donation) less negative the value of $\Delta E_{back\text{-}donation}$, better will be the corrosion inhibition efficiency. N-NLA 3 has a less negative, ΔE back-donation value, representing its maximum inhibition efficiency.

Frontier molecular orbital (FMO) can deliver theoretical results easily, according to the value of the energy gap between E_{HOMO} and E_{LUMO} ($\Delta E = E_{LUMO}$-E_{HOMO}). A high energy molecular orbital may tend to donate electrons to the acceptor with a low energy molecular orbital if the energy HOMO (E_{HOMO}) is high. The parameter energy LUMO (E_{LUMO}) refers to the ability to accept an electron from the molecule. Energy gap decreases increases the effectiveness of the inhibitor. In this study, the energy gap of N-NLA 3 is very low, which shows that it have good inhibitor efficiency.

5. Conclusion

DFT methods with the 6-311G basis set are used to analyze the vibrational frequencies of N_ω Nitro-L-Arginine. The vibrational frequencies of the fundamental modes of the molecule are assigned and analysed in detail. Experimental frequencies are associated with the theoretical results. FTIR, UV, NMR and quantum chemical calculations were made on the title compound to identify its structure, vibrational wave number, absorption wavelength, electronic properties, and chemical shift values which agree well with the experimental results. Theoretically, optimized parameters such as bond length, bond angle and dihedral angle are assessed and contrasted. The electric field effect is observed in the HOMO–LUMO gaps of Nω-Nitro-L-Arginine. The experimental vibrational spectrum analysis for N-NLA has been performed. As the electric field increases, the HOMO–LUMO gap decreases greatly from 4.7804 eV to 00.3234 eV. The first hyperpolarizabilities of Nω Nitro-L-Arginine is 3.5250×10^{-30} esu, respectively. The global reactivity descriptors parameters are calculated and explained in terms of the solvent. The energy gap between HOMO and LUMO indicates the ultimate charge transfer interactions which take place inside a molecule. DFT Mulliken charges gave a correct assessment of electrophilic and nucleophilic reactivity. The electrostatic potential surface gave a visual representation of the chemically active spots and their comparative reactivity of atoms. From TDDFT method, the absorption wavelength, oscillator strength, and excitation energies of the title compound are also calculated and compared with experimental values. DFT calculations at B3LYP/6-311G basis set level have been used to elucidate the inhibitor properties of title compound with various donors. Due to the highest HOMO energy and ΔN values, N-NL3 had the best corrosion inhibitor performance due to its ability to offer electrons and least energy gap.

Declaration of competing interest

There is no conflict of interest.

Acknowledgement

We thank Cauvery College for Women (Autonomous), Tiruchirappalli, for providing instrument facility under the support of DST-FIST-Level 0 program (Ref. No. SR/FST/College-246/2015(c)).

References

[1] M. Akram, H.M. Asif, M. Uzair, Naveed Akhtar, Asadullah Madni, S.M. Ali Shah Zahoorul Hasan1, Asmat Ullah, Amino acids: a review article, J. Med. Plants Res. 5 (17) (2011) 3997–4000, https://doi.org/10.5897/JMPR.9000061.

[2] H.D. Ashmead, The Role of Amino Acid Chelates in Animal Nutrition, Noyes Publications, Westwood, 1993.

[3] W. Leuchtenberger, K. Huthmacher, K. Drauz, Biotechnological production of amino acids and derivatives: current status and prospects, Appl. Microbiol. Biotechnol. 69 (1) (2005) 1–8, https://doi.org/10.1007/s00253-005-0155-y.

[4] Agnieszka Wojciechowskaa, Janczakb Jan, Wiktor Zierkiewicza, , Piotr Rytlewskic Tomasz Rojeka, Marek Duczmal, Copper(II) complex with L-arginine – crystal structure, DFT calculations, spectroscopic, thermal and magnetic properties Materials Chemistry and Physics, Mater. Chem. Phys. 228 (2019) 272–284, https://doi.org/10.1016/j.matchemphys.2019.02.037.

[5] A. Yokotani, T. Sasaki, K. Yoshida, S. Nakai, Efficient stimulated Brillouin scattering in the organic crystal deuterated L-arginine phosphate monohydrate Appl, Phys. Lett. 55 (1989) 2692–2693, https://doi.org/10.1364/JOSAB.15.000446.

[6] V. Natarajan, M. Arivanandhan, K. Sankaranarayanan, P. Ramasamy, Growth aspects and characteristic properties of pure and Li-doped L-arginine acetate (LAA) single crystals: a promising, J. Cryst. Growth 311 (2009) 572–575.

[7] Z.H. Sun, G.H. Zhang, X.Q. Wang, Z.L. Gao, X.F. Cheng, S.J. Zhang, D. Xu, Growth, morphology, thermal, spectral, linear, and nonlinear optical properties of L-arginine bis(trifluoroacetate) crystal, Cryst. Growth Des. 9 (2009) 3251–3259, https://doi.org/10.1021/cg801360.q.

[8] Z.H. Sun, W.M. Sun, C.T. Chen, G.H. Zhang, X.Q. Wang, D. Xu, L-arginine trifluoroacetate salt bridges in its solid state compound: the low-temperature three dimensional structural determination of L-arginine bis(trifluoroacetate) crystal and its vibrational spectral analysis Spectrochim, Acta, Part A: Mol. Biomol. Spectrosc 83 (2011) 39–45, https://doi.org/10.1016/j.saa.2011.07.008.

[9] P.K. Moore, O.A. Al-Swayeh, N.W.S. Chong, R.A. Evans, A. Gibson, L-NG-nitro arginine (L-NOARG), a novel, L-arginine-reversible inhibitor of endothelium-dependent vasodilatation in vitro, British, J. Pharmacol. 99 (2) (1990) 408–412, https://doi.org/10.1111/j.1476-5381.1990.tb14717.x.

[10] M. Bansinath, B. Arbabha, H. Turndorf, U.C. Garg, Chronic administration of a nitric oxide synthase inhibitor, N^{ω}-nitro-L-arginine, and drug-induced increase in cerebellar cyclic GMP in vivo, Neurochem. Res. 18 (10) (1993) 1063–1066, https://doi.org/10.1007/BF00966685.

[11] M.J. Frisch, G.W. Trucks, H.B. Schlegal, et al., GAUSSIAN 09, Revision A.02, Gaussian, Inc., Wallingford CT, 2009.

[12] O.L. Woodman, G.J. Dusting, N-nitro L-arginine causes coronary vasoconstriction and inhibits endothelium-dependent vasodilatation in anaesthetized greyhounds, Br. J. Pharmacol 103 (2) (1991) 1407–1410, https://doi.org/10.1111/2Fj.1476-5381.1991.tb09802.x.

[13] V. Karunakaran, V. Balachandran, FT-IR, FT-Raman spectra, NBO, HOMO–LUMO and thermodynamic functions of 4-chloro-3-nitrobenzaldehyde based on ab initio HF and DFT calculations, Spectrochim. Acta Part A: Mol. and Bio. Mol. Spec. 98 (2012) 229–239, https://doi.org/10.1016/j.saa.2012.08.003.

[14] O. Hernandez, K.S. Knight, W. Van Beek, A. Boucekkine, A. Boudjada, W. Paulus, J. Meinnel, IV of 1,3,5-trichloro-2,4,6-trimethylbenzene: ab initio crystal structure determination by high-resolution powder diffraction, J. Mol. Struct 791 (2006) 41–52, https://doi.org/10.1016/j.molstruc.2006.01.014.

[15] M. Govindarajan, M. Karabacak, Spectroscopic properties, NLO, HOMO–LUMO and NBO analysis of 2,5-Lutidine, Spectrochim. Acta Part A: Mol. and Bio. Mol. Spec. 96 (2012) 421–435, https://doi.org/10.1016/j.saa.2012.05.067.

[16] P. Srinivasan, Y. Vidyalakshmi, R. Gopalakrishnan, A highly efficient organic nonlinear optical donor- acceptor single crystal: L-valinium picrate, Cryst. Growth Des. 8 (7) (2008) 2340–2345, https://doi.org/10.1021/cg701143n.

[17] L.N. Wang a, X.Q. Wang a, G.H. Zhang a, X.T. Liu a, Z.H. Sun b, G.H. Sun a, L. Wang a, W.T. Yu a, D. Xu a, Single crystal growth, crystal structure and characterization of a novel crystal: L-arginine 4-nitrophenolate 4-nitrophenol dehydrate (LAPP), J. Cryst. Growth 327 (2011) 133–139, https://doi.org/10.1016/j.jcrysgro. 2011.05.010.

[18] Mohd Shkira, S. Al Faifya, Haider Abbasb, S. Muhammada, First principal studies of spectroscopic (IR and Raman, UV-visible), molecular structure, linear and nonlinear optical properties of L-arginine p-nitrobenzoate monohydrate (LANB): a new non-centro symmetric material, Spectrochim. Acta Mol. Biomol. Spectrosc. (2015) 1–30, https://doi.org/10.1016/j.saa.2015.02.111.

[19] C. Usha, R. Santhakumari, Lynnette Joseph, D. Sajan c, R. Meenakshi, A. Sinthiya, Growth and combined experimental and quantum chemical study of glycyl-LValine crystal, Heliyon (2019), https://doi.org/10.1016/j.heliyon.2019.e01574, 1-24.

[20] S. Arunaa, A. Anuradhab, Preema C. Thomas, M. Gulam Mohamedc, S. A. Rajasekard, M. Vimalan, G. Mani, P. Sagayaraj, Growth, optical and thermal studies of L-arginine perchlorate - a promising non-linear optical single crystal, Indian J. Pure Appl. Phys. 45 (6) (2007) 524–552. http://nopr.niscair.res.in/handle/123456789/2525.

[21] Piotr Rejnhardt, Marek Daszkiewicz, Crystal structure, theoretical and vibrational analysis of isostructural salts of L-arginine analogue, (S)-2-amino-3-guanidinopropanoic acid, J. Mol. Struct. (2020) 1–9, https://doi.org/10.1016/j.molstruc.2020.129620.

[22] Pradyot Patnaik, Dean, Analytical Chemistry Handbook, McGraw-Hill, New York, 1995, ISBN 9780071410601.

[23] N.B. Colthup, L.H. Daly, S.E. Wiberley, Introduction to Infrared and Raman Spectroscopy, Academic Press, New York, 1964, ISBN 9780080917405 eBook ISBN:.

[24] M. Silverstein, G.C. Basseler, C. Morill, Spectrometric Identification of Organic Compounds, Wiley, New York, 2001, https://doi.org/10.1002/oms.1210260923.

[25] S. Sivaprakasha, S. Prakashb, S. Mohanc Sujin, P. Jose, Quantum chemical studies and spectroscopic investigations on 2-amino-3-methyl-5-nitropyridine by density functional theory 5(7), (2019), 1-10, https://doi.org/10.1016/j.heliyon. 2019.e02149.

[26] Emine Tanış, Nevin Çankaya, Serap Yalçın, Synthesis, Characterization, computation of global reactivity descriptors and antiproliferative activity of *N*-(4-nitrophenyl)Acrylamide, Russ. J. Phys. Chem. B 13 (No. 1) (2019) 49–61, https://doi.org/10.1134/S1990793119010147.

[27] Sefa Celik, Aysen E. Ozel, Volkan Durak, Sevim Akyuz, Vibrational spectroscopic characterization, quantum chemical and molecular docking studies of Valyl-Methionine dipeptide, Spectros. Let. (2020) 648–663, https://doi.org/10.1080/00387010.2020.1821062.

[28] S. Muthu, M. Prasath, R. Balaji, Experimental and theoretical investigations of spectroscopic properties of 8-chloro-1-methyl-6-phenyl-4H-[1,2,4] triazolo [4,3-a]

[1,4] benzodiazepine, Spectrochim. Acta Mol. Biomol. Spectrosc. 106 (2013) 129–145, https://doi.org/10.1016/j.saa.2012.12.057.
[29] N. Bakiler, I.V. Maslov, S. Akyuz, Theoretical study of the vibrational spectra of 2-chloropyridine metal complexes. I. Calculation and analysis of the IR spectrum of 2-chloropyridine, J. Mol. Struct. 475 (1999) 83–92, https://doi.org/10.1016/S0022-2860(98) 00491-8.
[30] T. Prabhu, S. Periandy, S. Ramalingam, FT-IR and FT-Raman spectroscopic investigation, computed vibrational frequency analysis and IR intensity and Raman activity peak resemblance analysis on 2-nitroanisole using HF and DFT (B3LYP and B3PW91) calculations, Spectrochim. Acta, Part A 83 (1) (2011) 8–16, https://doi.org/10.1016/j.saa.2011.04.004.
[31] M. Govindarajan, M. Karabacak, Analysis of vibrational spectra (FT-IR and FT-Raman) and nonlinear optical properties of organic 2-chloro-p-xylene Spectrochim, Acta 94 (2012) 36–47, https://doi.org/10.1016/j.saa.2012.03.043.
[32] P. Vinnarasia, M. Victor Antony Raja, b J. Madhavana, Growth and characterization of nonlinear optical crystal L-isoleucine D-norleucine: a DFT approach, Mater. Today Proc. 8 (2019) 492–501, https://doi.org/10.1016/j.matpr.2019.02.143.
[33] S. Ranjitha a, V. Aroulmoji b, T. Mohrb c, P.M. Anbaras, G. Rajarajane, Acta Phys. Pol., A 126 (2014) 833–839.
[34] Weitao Yang, *Ab initio* approach for many-electron systems without invoking orbitals: an integral formulation of density-functional theory, Phys. Rev. Let. 59 (1987) 1569, https://doi.org/10.1103/PhysRevLett. 59.1569.
[35] R. Meenakshi, Spectral investigations, DFT based global reactivity descriptors, Inhibition efficiency and analysis of 5-chloro-2-nitroanisole as π-spacer with donor-acceptor variations, J. Mol. Struct. 1127 (2017) 694–707, https://doi.org/10.1016/j.molstruc.2016.08.030.
[36] R. Meenakshi, FT-IR and FT-Raman analysis and light-harvesting efficiency (LHE) enhancement for DSSC applications of hydrazide derivatives, J. Iran. Chem. Soc. 8 (5) (2021) 1179–1198, https://doi.org/10.1007/s13738-020-02101-y.
[37] Gokhan Gece, The use of quantum chemical methods in corrosion inhibitor studies, Corrosion Sci. 50 (2008) 2981–2992, https://doi.org/10.1016/j.corsci.2008.08.043.
[38] Y. Ye, M. Zhang, J. Zhao, Ab inito investigations on three isomers of polyacetylene under the interaction of external electric field, J. Mol. Struct. 822 (2007) 12–20, https://doi.org/10.1016/j.theoche.2007.07.007.
[39] A. David Stephen, Reji Thomas, P. Srinivasan, N. Vijayan, P. Kumaradhas, Exploring the bond topological and electrostatic properties of benzimidazole molecule via experimental and theoretical charge density study, J. Mol. Struct. 989 (2011) 122–130, https://doi.org/10.1016/j.molstruc.2011.01.014.
[40] R.G. Pearson, Chemical hardness and density functional theory, J. Chem. Sci. 117 (2005) 369–377, https://doi.org/10.1007/BF02708340.
[41] R.G. Pearson, Absolute electronegativity and hardness: application to inorganic chemistry, Inorg. Chem. 27 (4) (1988) 734–740, https://doi.org/10.1021/ic00277a030.
[42] Ahmed H. Radhi, A.B. Ennas, Fatma Du, A. Khazaal, Zaid M. Abbas, Oday H. Aljelawi, Salam D. Hamadan, Haider A. Almashhadani, Mustafa M. Kadhim, HOMO-LUMO energies and geometrical structures effecton corrosion inhibition for organic compounds predict by DFT and PM3 methods, NeuroQuantology 18 (2020) 37–45, https://doi.org/10.14704/nq.2020.18.1.NQ20105.
[43] P. Politzer, J. Murray, D.L. Beveridge, R. Lavery (Eds.), Theoretical Biochemistry and Molecular Biophysics: A Comprehensive Survey, vol. 2, Adenine Press, Schenectady, NY, 1991 (Chapter 13).
[44] P. Politzer, J. Murray, The fundamental nature and role of the electrostatic potential in atoms and molecules, Theo. Chem. Acc. 108 (2002) 134–142, https://doi.org/10.1007/s00214-002-0363-9.
[45] Kadali Chaitanya, Xue-Hai Ju, B. Mark Heron, Theoretical study on the light harvesting efficiency of zinc porphyrin sensitizers for DSSCs, RSC Adv. 4 (2014) 26621–26634, https://doi.org/10.1039/C4RA02473G.
[46] B. Kosar, C. Albayrak, Spectroscopic investigations and quantum chemical computational study of (E)-4-methoxy-2-[(p-tolylimino) methyl]phenol, Spectrochim. Acta 78 (2011) 160, https://doi.org/10.1016/j.saa.2010.09.016.
[47] P.W. Atkins, Physical Chemistry, Oxford University Press, Oxford, 2001, ISBN 0-7167-8759-8. EAN: 9780716787594.
[48] E.A. Yaqo, R.A. Anaee, M.H. Abdulmajeed, I.H. Tomi, M.M. Kadhim, Aminotriazole derivative as anti-corrosion material for Iraqi kerosene tanks: electrochemical, computational and the surface study, electrochemical, computational and the surface study, ChemistrySelect 4 (34) (2019) 9883–9892, https://doi.org/10.1002/slct.201902398.
[49] Bhawna Chugh, Ashish K. Singh, Sanjeeve Thakur, Balaram Pani, Hassane Lgaz, Ill-min Chung, Ranjana Jha, Ranjana Jha, Eno E. Ebenso, Comparative investigation of corrosion-mitigating behavior of thiadiazole-derived bis-schiff bases for mild steel in acid medium, Experimental, Theoretical, and Surface Study 5 (23) (2020) 13503–13520, https://doi.org/10.1021/acsomega. 9b04274.
[50] Dharmendr Kumara, Nimesh Jainb, Vinay Jaina, Beena Raia, Amino acids as copper corrosion inhibitors: a density functional theory approach, Appl. Surf. Sci. 514 (2020) 145905, https://doi.org/10.1016/j.apsusc.2020.145905.
[51] R.M. Issa, M.K. Awad, F.M. Atlam, Quantum chemical studies on the inhibition of corrosion of copper surface by substituted uracils, Appl. Surf. Sci. 255 (2008) 2433, https://doi.org/10.1016/j.apsusc.2008.07.155.
[52] P. Udhayakalaa, T.V. Rajendiranb, S. Gunasekaranc, Theoretical approach to the corrosion inhibition efficiency of some pyrimidine derivatives using DFT method, J. Comput. Methods Mol. Des. 2 (1) (2012) 1–15. ISSN: 2231- 3176.
[53] H. Nwankwo, L. Olasunkanmi, E. Ebenso, Experimental, quantum chemical and molecular dynamic simulations studies on the corrosion inhibition of mild steel by some carbazole derivatives Sci, For. Rep. 7 (2017) 2436, https://doi.org/10.1038/s41598-017-02446-0.